

# On the possibility of search for $L_\mu - L_\tau$ gauge boson at Belle-II and neutrino beam experiments

Yuya Kaneta<sup>1,\*</sup> and Takashi Shimomura<sup>2,†</sup>

<sup>1</sup>*Graduate School of Science and Technology,  
Niigata University, Niigata 950-2181, Japan*

<sup>2</sup>*Faculty of Education, Miyazaki University, Miyazaki, 889-2192, Japan*

(Dated: February 16, 2022)

## Abstract

We study the possibilities on the search of the light and weakly interacting gauge boson in the gauged  $L_\mu - L_\tau$  model. Introducing the kinetic mixing at the tree-level, the allowed parameter regions for the gauge coupling and kinetic mixing parameter are presented. Then, we analyze one photon plus missing event within the allowed region and show that search for the light gauge boson will be possible at Belle-II experiment. We also analyze neutrino trident production process in neutrino beam experiments.

---

\*Electronic address: kaneta@muse.sc.niigata-u.ac.jp

†Electronic address: shimomura@cc.miyazaki-u.ac.jp

## I. INTRODUCTION

The anomalous magnetic moment of the muon,  $(g-2)_\mu$ , is one of the most precisely measured and calculated quantities in particle physics. Therefore it can provide a sensitive search for new physics beyond the Standard Model (SM). Over recent decades, there has remained a discrepancy between experimental values [1, 2] and the SM predictions [3–6],

$$\Delta a_\mu \equiv a_\mu^{\text{exp}} - a_\mu^{\text{theo}} = (28.8 \pm 8.0) \times 10^{-10}, \quad (1)$$

which corresponds to  $3.6\sigma$  deviation from the SM prediction. The discrepancy can be verified in forthcoming experiments that will reduce the uncertainties by about a factor of four [7, 8]. If the discrepancy is confirmed by the experiments, it will be a clear evidence of new physics beyond the SM.

On theoretical side, many extensions of the SM have been proposed to explain this discrepancy so far (see [9, 10] for review and [11] for recent works). Among them, new  $U(1)$  gauge symmetries are of particular interest since these are one of the minimal extensions of the SM. To resolve the discrepancy of  $(g-2)_\mu$  in this class of models, the simplest possibility is that muons are charged under the new symmetry while other SM particles are neutral. Then, the muon receives a contribution from the new gauge boson to its anomalous magnetic moment. For the  $U(1)$  symmetry to be anomaly-free, the condition,  $3B = L_e + L_\mu + L_\tau$ , must be satisfied where  $B$  is the baryon number and  $L_{e,\mu,\tau}$  are the flavour numbers, respectively.

Among anomaly free  $U(1)$  symmetries, the  $L_\mu - L_\tau$  symmetry is particularly interesting [12–14]. The models with the  $L_\mu - L_\tau$  symmetry can provide the large atmospheric mixing as the leading approximation, with some extensions such as adding right-handed neutrinos and new scalar particles to obtain the correct reactor angle of the lepton mixing [15–21], and these also can explain the gap in the cosmic neutrino spectrum observed by IceCube [22–25]. Furthermore, when the interactions between quarks and the gauge boson associated with the symmetry are introduced, the models can explain the anomalies reported by LHCb [26–28]. Recent studies in the model can be found for neutrino trident production processes [29, 30], rare Kaon decays [31], lepton flavour violations [32] and related phenomenologies [20, 21, 33–35]. For direct and indirect searches of such the gauge boson, new experiments are under preparation [36–38]. In the previous studies, the result of [29] showed the gauge boson mass and the coupling constant must be lighter than 400 MeV and smaller than  $10^{-3}$  without kinetic mixing model. Such the light and weakly interacting gauge boson will be difficult to search in high energy experiments because its production cross sections and decay branching ratios are very suppressed. Therefore, high-luminosity or high-flux experiments like the Belle-II and neutrino oscillation experiments are suitable for the search of such the gauge boson.

The search of light and weakly interacting gauge bosons at the Belle-II experiment has been studied in the context of the dark photon scenario [39, 40], where the SM fermions interact with the dark photon only through the kinetic mixing with the photon. On the other

	$l_\mu = (\nu_\mu, \mu_L)^T$	$l_\tau = (\nu_\tau, \tau_L)^T$	$\mu_R$	$\tau_R$
$U(1)_{L_\mu-L_\tau}$	1	-1	1	-1

TABLE I: The charge assignment of gauged  $U(1)_{L_\mu-L_\tau}$  model. Here,  $l_\mu$  and  $l_\tau$  represent  $SU(2)$  doublets, and  $\mu_R$  and  $\tau_R$  represent  $SU(2)$  singlets of muon and tau flavours, respectively. All other SM fermions and the Higgs are singlet under this symmetry.

hand, in the studies on  $L_\mu - L_\tau$  models mentioned above, the kinetic mixing at tree-level is usually set to be zero by hand. Such the tree-level kinetic mixing, however, is allowed by the symmetries and therefore should be considered simultaneously. In this paper, we consider a model with the gauged  $U(1)_{L_\mu-L_\tau}$  symmetry in the presence of the kinetic mixing, and explore the allowed parameter space for the light and weakly interacting gauge boson. Then, we study the possibilities of search for such the gauge boson in one-photon plus missing event at the Belle-II experiment, and in the neutrino trident production process at neutrino beam experiments.

This paper is organized as follows. In section II, we introduce the model with the gauged  $U(1)_{L_\mu-L_\tau}$  symmetry, and show the relevant interactions and decay widths of the  $L_\mu - L_\tau$  gauge boson. In section III, the experimental constraints and requirements to restrict the model parameters are explained. Then, in section IV, we show the allowed parameter regions of the model. In section V, the possibilities of search for the gauge boson at Belle-II and neutrino beam experiments are discussed. Section VI is devoted to summary and discussions.

## II. GAUGED $L_\mu - L_\tau$ MODEL

We start our discussion with introducing our model. The SM is extended by adding the gauged  $U(1)_{L_\mu-L_\tau}$  symmetry under which muon and tau flavour leptons are charged. The charge assignment of the symmetry is summarized in Table I. Here  $l_\mu$  and  $l_\tau$  represent  $SU(2)$  doublets, and  $\mu_R$  and  $\tau_R$  represent  $SU(2)$  singlets of muon and tau flavours, respectively. Then, the Lagrangian of the model takes the form of

$$\mathcal{L} = \mathcal{L}_{\text{SM}} - V_{L_\mu-L_\tau} - \frac{1}{4}Z'_{\mu\nu}Z'^{\mu\nu} + \frac{\epsilon}{2}B_{\mu\nu}Z'^{\mu\nu} + g'Z'_\mu J^\mu_{Z'}, \quad (2)$$

$$J^\mu_{Z'} = \bar{l}_\mu \gamma^\mu l_\mu + \bar{\mu}_R \gamma^\mu \mu_R - \bar{l}_\tau \gamma^\mu l_\tau - \bar{\tau}_R \gamma^\mu \tau_R, \quad (3)$$

where  $\mathcal{L}_{\text{SM}}$  and  $V_{L_\mu-L_\tau}$  stand for the SM Lagrangian and the scalar potential responsible for the  $L_\mu - L_\tau$  symmetry breaking, and  $Z'$  and  $B$  represent the gauge fields of the  $U(1)_{L_\mu-L_\tau}$  and the hypercharge  $U(1)_Y$ , respectively. The same symbols for their field strengths are used. The gauge coupling constant and the kinetic mixing parameter are denoted as  $g'$  and  $\epsilon$ , and the  $U(1)_{L_\mu-L_\tau}$  current,  $J^\mu_{Z'}$ , is given by Eq.(3). In this work, we concentrate our discussion on the gauge sector and hence do not specify the potential  $V_{L_\mu-L_\tau}$ . We assume that the

$L_\mu - L_\tau$  symmetry is spontaneously broken without conflicting experimental constraints such as the SM Higgs couplings to the SM gauge bosons<sup>1</sup>. Therefore, we treat the mass of  $Z'$ ,  $m_{Z'}$ , as a free parameter.

After the electroweak and  $L_\mu - L_\tau$  symmetries are broken down, the gauge bosons acquire the masses and their neutral components mix each other due to the kinetic mixing. Then the interaction Lagrangian of leptons with the gauge bosons in mass-basis is obtained by diagonalizing their kinetic terms as well as mass terms. Assuming  $m_{Z'}$  is much lighter than the  $Z$  boson mass, the interaction Lagrangian is given by

$$\mathcal{L}_{\text{int}} = eA_\mu J_{\text{EM}}^\mu + g_2 Z_\mu J_{\text{NC}}^\mu + Z'_\mu (e\epsilon \cos \theta_W J_{\text{EM}}^\mu + g' J_{Z'}^\mu) + \mathcal{O}(\epsilon^2), \quad (4)$$

where  $J_{\text{EM}}^\mu$  and  $J_{\text{NC}}^\mu$  are the electromagnetic and weak neutral currents of the SM, respectively, and  $e$  and  $\theta_W$  are the electric charge and the Weinberg angle. In Eq. (4), we have neglected the terms of order  $\epsilon^2$  and higher order ones. Such the terms include the interaction of electron neutrinos with  $Z'$ . As we will show in the following sections, the kinetic mixing parameter and the gauge coupling constant of our interest are smaller than  $10^{-3}$ . Therefore, these terms can be safely ignored in our discussion. The kinetic mixing also can be generated via muon and tau loops, which is two orders of magnitude suppressed than  $g'$ . We also ignore such the kinetic mixing for simplicity.

The decay widths of  $Z'$  are given by,

$$\Gamma(Z' \rightarrow \nu \bar{\nu}) = \frac{g'^2}{24\pi} m_{Z'}, \quad (5a)$$

$$\Gamma(Z' \rightarrow e^+ e^-) = \frac{(\epsilon e \cos \theta_W)^2}{12\pi} m_{Z'} \sqrt{1 - \frac{4m_e^2}{m_{Z'}^2}} \left(1 + \frac{2m_e^2}{m_{Z'}^2}\right), \quad (5b)$$

$$\Gamma(Z' \rightarrow l^+ l^-) = \frac{(g' \mp \epsilon e \cos \theta_W)^2}{12\pi} m_{Z'} \sqrt{1 - \frac{4m_l^2}{m_{Z'}^2}} \left(1 + \frac{2m_l^2}{m_{Z'}^2}\right), \quad (5c)$$

$$\Gamma(Z' \rightarrow \text{hadrons}) = \frac{(\epsilon e \cos \theta_W)^2}{12\pi} m_{Z'} \sqrt{1 - \frac{4m_\mu^2}{m_{Z'}^2}} \left(1 + \frac{2m_\mu^2}{m_{Z'}^2}\right) R(s = m_{Z'}^2), \quad (5d)$$

where  $l = \mu, \tau$  and the sign in Eq. (5c) is  $-$  for  $\mu$  and  $+$  for  $\tau$ , respectively. In Eq. (5d),  $R(s)$  is the  $R$ -ratio defined by  $\sigma_{e^+ e^- \rightarrow \text{hadrons}} / \sigma_{e^+ e^- \rightarrow \mu^+ \mu^-}$  and can be found in [2]. For  $\sqrt{s} \lesssim 0.36$  GeV, we use the cross section for  $e^+ + e^- \rightarrow \pi^+ + \pi^-$  [41, 42]. The branching ratio of  $Z' \rightarrow \nu + \bar{\nu}$  obtained from Eqs. (5) is used in the following analyses.

---

<sup>1</sup> This assumption can be realized when we introduce a scalar  $S$  which is singlet under the SM gauge symmetries. Such the scalar has a quartic interaction with the SM Higgs,  $|S|^2 |H|^2$ . However, their mixing can be very small by taking the quartic coupling enough small.

### III. EXPERIMENTAL CONSTRAINTS

In this section, we explain experimental bounds and requirements to constrain the parameters of the model,  $g'$ ,  $\epsilon$  and  $m_{Z'}$ .

#### A. Muon anomalous magnetic moment

As mentioned in the introduction, muons receive contributions from  $Z'$  to its anomalous magnetic moment. At the one-loop level, the contribution is given by

$$\Delta a_\mu^{Z'} = \frac{(g' - \epsilon e \cos \theta_W)^2}{8\pi^2} \int_0^1 dx \frac{2m_\mu^2 x^2 (1-x)}{x^2 m_\mu^2 + (1-x)m_{Z'}^2}, \quad (6)$$

where  $m_\mu$  is the mass of a muon. We require the contribution Eq.(6) to be within  $2\sigma(3\sigma)$ , that leads to

$$12.8 \text{ (4.8)} \lesssim \Delta a_\mu^{Z'} \times 10^{10} \lesssim 44.8 \text{ (52.8)}. \quad (7)$$

#### B. Neutrino trident production process

The neutrino trident production process is the scattering of a muon neutrino off the Coulomb field of a nucleus ( $N$ ), producing two muons in the final state,  $\nu_\mu + N \rightarrow \nu_\mu + \mu^+ + \mu^- + N$ . This process can occur both in the SM and in the  $L_\mu - L_\tau$  model. The process offers a sensitive search for the light  $Z'$  boson as shown in [29, 30] since the SM contributions are much suppressed due to the weak interaction. The experimental search results have been reported by CCFR [43] and CHARM-II [44] collaborations, and the most stringent bound was set by the CCFR experiment,

$$R_{\text{CCFR}} \equiv \frac{\sigma_{\text{CCFR}}}{\sigma_{\text{SM}}} = 0.82 \pm 0.28. \quad (8)$$

In [29], it was shown that the favored parameter region of  $(g-2)_\mu$  is excluded for  $m_{Z'} \gtrsim 400$  MeV without the kinetic mixing in the  $L_\mu - L_\tau$  model. In Sec. IV, we calculated the trident production cross section under the equivalent photon approximation [45, 46] using CalcHEP [47] for photon-neutrino scattering cross section. We found that our cross sections and results are in good agreement with [48] and [29]. We require the  $Z'$  contribution should be less than 95% C.L. of Eq. (8).

#### C. Neutrino-electron scatterings

Neutrino-electron scattering tightly constrains  $g'$  and  $\epsilon$  for a dark photon and a light  $Z'$  boson [49, 50]. To our model, the constraints from reactor neutrino experiments, e.g. the

TEXONO experiment [51–54], are irrelevant because the interaction of electron neutrinos with  $Z'$  is negligibly small. Then, the most stringent constraints come from the Borexino experiment [55] that has measured the solar neutrinos. The  ${}^7\text{Be}$  neutrinos, which is  $\nu_e$ , oscillate to  $\nu_\mu$  and  $\nu_\tau$  on the way to the Earth and therefore are scattered by electron via  $Z'$  exchange. In [49], the constraint from Borexino in a  $U(1)_{B-L}$  model was studied. We translate the constraint given in [49]<sup>2</sup> using

$$g_{B-L} > \left[ (\epsilon e \cos \theta_W)^2 \sum_{j=1}^3 f_i |g_{ij}|^2 \right]^{1/4}, \quad (9)$$

$$|g_{ij}| \equiv |g'(V^\dagger Q V)_{ij}| = g' \begin{pmatrix} 0.051 & 0.158 & 0.556 \\ 0.158 & 0.082 & 0.808 \\ 0.556 & 0.808 & 0.133 \end{pmatrix}, \quad (10)$$

where  $V$  is the lepton mixing matrix [56, 57] and  $Q = \text{diag}(0, 1, -1)$  is the  $L_\mu - L_\tau$  charge matrix,  $f_i$  stands for the fraction of  $i$ -th mass eigenstate of  ${}^7\text{Be}$  neutrinos at the Earth [58]. Here, we assumed the normal hierarchy of neutrino mass spectrum [2]<sup>3</sup>.

#### D. Beam dump experiment

Dark photon searches at electron beam dump experiments, such as E141 [59] and U70 [60] also restrict the model parameters. The coupling constant and kinetic mixing parameter are allowed when the  $Z'$  boson decays in a beam dump before it reaches to a detector or it is long-lived so that it penetrates a detector. The latter case corresponds to too small coupling constant and kinetic mixing which can not explain  $(g - 2)_\mu$ . Therefore we consider the former case. The constraint can be translated from the study in the dark photon scenario [61] by

$$\frac{|\epsilon \cos \theta_W|}{\sqrt{\text{Br}(Z' \rightarrow e^+ e^-)}} \gtrsim \epsilon_{\text{BD}}, \quad (11)$$

where  $\epsilon_{\text{BD}}$  is the kinetic mixing parameter for the dark photon given in [61].

#### E. Meson decay experiment

Another dark photon searches were performed at the NA48/2 [62] and E787, E949 [63, 64] experiments in which the signals of the dark photon production were searched from the decays of pion and kaon, respectively. There analyzed the dark photon decay into an

<sup>2</sup> The constraint including the interference effect was studied in [50], which showed the constraint is improved by about 30%. This effect is important and will be included in our next work.

<sup>3</sup> This constraint is almost the same for the inverted hierarchy case.

electron and a positron in NA48/2 while the decay into invisible particles in E787/E949. The constraints from these experiments give similar bounds and hence we employ the NA48/2 result<sup>4</sup>. Then, the constraint can be translated using

$$|\epsilon \cos \theta_W| \sqrt{\text{Br}(Z' \rightarrow e^+ e^-)} \lesssim \epsilon_{\text{MD}}, \quad (12)$$

where  $\epsilon_{\text{MD}}$  is the kinetic parameters given in [62].

### F. Electron-Positron Collider Experiment

The  $Z'$  boson can be directly produced in  $e^+ e^-$  collision via the kinetic mixing. The searches for a light gauge boson such as the dark photon have been performed in  $e^+ e^-$  collider [66, 67], and the most stringent bound is set by the BaBar experiment [68]. The  $Z'$  boson can decay into charged leptons and be detected as  $e^+ + e^- \rightarrow \gamma + l^+ + l^-$  ( $l = e, \mu$ ). The constraint can be translated using

$$|\epsilon \cos \theta_W| \sqrt{\text{Br}(Z' \rightarrow l^+ l^-)} \lesssim \epsilon_{\text{BaBar}}, \quad (13)$$

where  $\epsilon_{\text{BaBar}}$  is the kinetic mixing parameters in the dark photon given in [68]. Furthermore, the constraint for  $m_{Z'} > 2m_\mu$  in the  $L_\mu - L_\tau$  model without the kinetic mixing was reported in [69] by searching the decay of  $Z'$  into muons.

### G. Electron anomalous magnetic moment

The  $Z'$  boson also contributes to the magnetic moment of the electron at the one-loop level similar to the muon. The contribution can be obtained by simply setting  $g' = 0$  and replacing  $m_\mu$  with the electron mass in Eq. (6). We require that the  $Z'$  contribution to the electron magnetic moment  $(g - 2)_e$  should be within  $3\sigma$  [70, 71],

$$\Delta a_e \lesssim 13.8 \times 10^{-13}. \quad (14)$$

## IV. ALLOWED PARAMETER REGION

In this section, we show the allowed region of the parameter space in the  $g'$ - $\epsilon$  plane taking into account the constraints and requirements explained in Sec. III. Since the constraints and requirements depend on  $m_{Z'}$ , we choose  $m_{Z'} = 10, 50, 100$  and  $300$  MeV as illustrating examples.

---

<sup>4</sup> The NA64 collaboration recently reported the result of the dark photon search via invisible decays [65]. This result is similar to that from the BaBar experiment, and hence we do not consider in this paper.

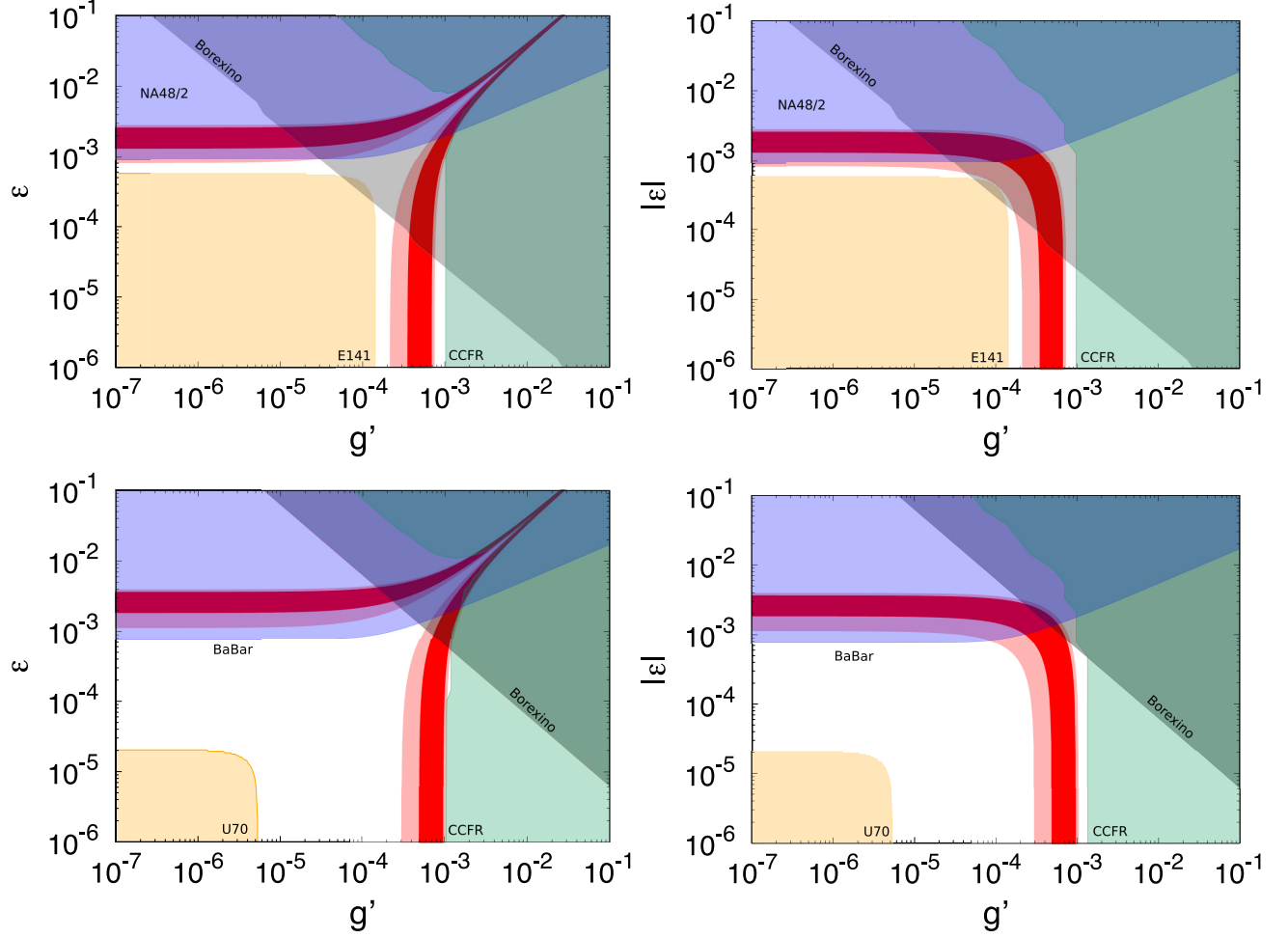


FIG. 1: The allowed region in the  $g'$ - $\epsilon$  plane. In the top and bottom panels,  $m_{Z'}$  is taken as 10 and 50 MeV, respectively, and in the left and right panels,  $\epsilon$  is positive and negative. The colored regions are excluded by the E141/U70 (yellow), the Borexino (grey), the CCFR (green) and  $(g-2)_e$  and/or the BaBar (blue) experiments. The red and pink bands correspond to  $2\sigma$  and  $3\sigma$  favored regions of  $(g-2)_\mu$ .

Figure 1 shows the allowed region in the  $g'$ - $\epsilon$  plane. The mass of  $Z'$  is taken as 10 MeV and 50 MeV for the top and bottom panels, and the kinetic mixing parameter is taken to be positive and negative for the left and right panels, respectively. In the figure, the yellow, grey and green regions are excluded by the E141/U70 (beam dump), the Borexino ( $\nu$ - $e$  scattering) and the CCFR (neutrino trident production) experiments. The blue region is also excluded by  $(g-2)_e$  and/or the BaBar ( $e^+e^-$  collider) and/or the NA48/2 (meson decay) experiment. The red and pink bands represent the favored regions of  $(g-2)_\mu$  within  $2\sigma$  and  $3\sigma$ , respectively. Figure 2 is the same plots for  $m_{Z'} = 100$  and 300 MeV.

From these figures, one can see that the  $(g-2)_\mu$  favored regions are different with the sign of  $\epsilon$ . In the case of positive  $\epsilon$  (left panels), the favored region of  $(g-2)_\mu$  is extended



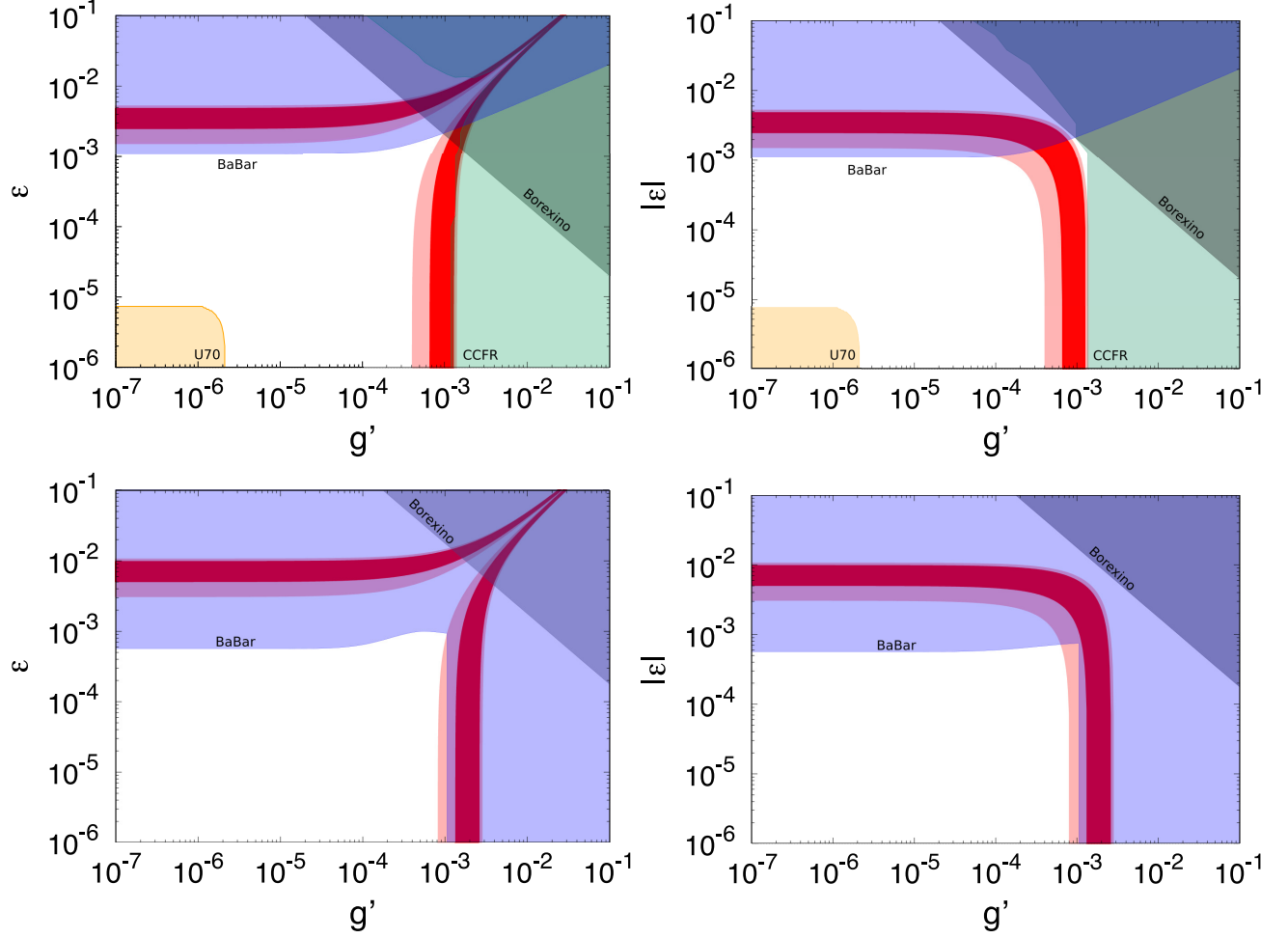


FIG. 2: The same plots as Figure 1 for  $m_{Z'} = 100$  (top) and 300 (bottom) MeV.

to the right-upper corner. This is because the coupling of the muon becomes smaller due to the cancellation between  $g'$  and  $\epsilon$ . In this region, the constraint from the CCFR experiment can be evaded. Then, slightly larger values of  $g'$  is allowed for  $m_{Z'} = 100$  MeV. In the case of negative  $\epsilon$  (right panels), on the other hand, the coupling becomes larger due to the addition of  $g'$  and  $\epsilon$ . One can also see that the constraint from CCFR is more stringent in negative  $\epsilon$  than in positive  $\epsilon$  for  $|\epsilon| \gg g'$ . In this parameter region, the coupling of the muon is given by  $-\epsilon \cos \theta_W$ , and therefore the relative phase of the amplitudes for the neutrino trident process is determined by the sign of  $\epsilon$ . Then, the amplitudes are added destructively for positive  $\epsilon$  while constructively for negative  $\epsilon$ . The difference of the excluded region by CCFR comes from this fact.

It is seen that, for  $g' \lesssim 10^{-4}$ , the BaBar or the NA48/2 experiments excludes the regions with roughly  $|\epsilon| \gtrsim 10^{-3}$  for  $m_{Z'} \lesssim 100$  MeV and  $|\epsilon| \gtrsim 5 \times 10^{-4}$  for  $m_{Z'} = 300$  MeV, respectively. Therefore,  $(g-2)_\mu$  can not be explained within  $3\sigma$  with  $g' \lesssim 10^{-4}$  for  $m_{Z'} \gtrsim 50$  MeV in our example parameters. This result generally holds for different values of  $m_{Z'}$  because

such the small  $g'$  does not change the constraint given in [62, 68]. On the other hand, for  $m_{Z'} = 10$  MeV, the allowed region including  $(g - 2)_\mu$  within  $3\sigma$  is found. One will find similar allowed regions for some values of  $m_{Z'} \lesssim 20$  MeV because the constraint from [62] becomes less stringent due to statistical fluctuations.

For  $|\epsilon| \lesssim 10^{-3}$ , it is seen that the regions with roughly  $g' \gtrsim 10^{-3}$  are excluded by the CCFR experiment for  $m_{Z'} \lesssim 100$  MeV and the BaBar experiment for  $m_{Z'} = 300$  MeV. For  $m_{Z'} = 10$  MeV, the E141 experiment also has excluded for  $g' \lesssim 1.3 \times 10^{-4}$ , and the Borexino has set the upper limit on  $\epsilon \lesssim 2 \times 10^{-4}$ . Then, the parameter space is much constrained, however  $(g - 2)_\mu$  within  $3\sigma$  is still allowed. For  $m_{Z'} \gtrsim 50$  MeV, the constraints from the beam dump experiments become weaker. These constraints come from that  $Z'$  is short lived so that it decays before reaching to a detector, as we mentioned in Sec. III. Since the lifetime is inversely proportional to the coupling constant squared times  $m_{Z'}$ , the coupling constant can be smaller as  $m_{Z'}$  is larger. This  $m_{Z'}$  dependence is incorporated in the values of  $\epsilon_{\text{BD}}$  given in [61]. The  $g'$  and  $\epsilon$  dependences of the excluded region can be understood by Eq. (11). For  $m_{Z'} = 300$  MeV, we superposed the constraint on  $g'$  (the vertical line) read from [69]. Strictly speaking, the constraint depends on  $\epsilon$ . However it may not be so different because  $g'$  is larger than  $\epsilon$  in this region.

## V. LIGHT $Z'$ SEARCH AT BELLE-II AND NEUTRINO BEAM EXPERIMENTS

Based on the results shown in Sec. IV, we study the possibilities on the search for the  $Z'$  boson at the Belle-II and neutrino beam experiments.

### A. The Belle-II experiment

The Belle-II experiment is an  $e^+e^-$  collider at the center of mass energy  $\sqrt{s} = 10.58$  GeV [72]. Its goal is to accumulate the integrated luminosity  $50 \text{ ab}^{-1}$  of  $e^+e^-$  collision data during by the middle of the next decade. In  $e^+e^-$  collision, the  $Z'$  boson can be produced through the kinetic mixing [73–75], and then decays into neutrinos, charged leptons and pions. The processes with charged leptons and pions in the final states will be overwhelmed by the SM backgrounds because those can occur by the electromagnetic interaction. The process with neutrinos, on the other hand, occurs by the weak interaction in the SM, and it is suppressed by the  $W$  and  $Z$  boson mass. Therefore the signal can be comparable to or larger than the background. Furthermore, the signal of the  $Z'$  production can be characterized by the energy of an associated photon.<sup>5</sup> The energy of the photon is given by

$$E_\gamma = \frac{4E_{e^+}E_{e^-} - m_{Z'}^2}{2(E_{e^+} + E_{e^-} + (E_{e^+} - E_{e^-}) \cos \theta_\gamma)}, \quad (15)$$

<sup>5</sup> A similar searched was done at BaBar for a pseudo scalar [76].

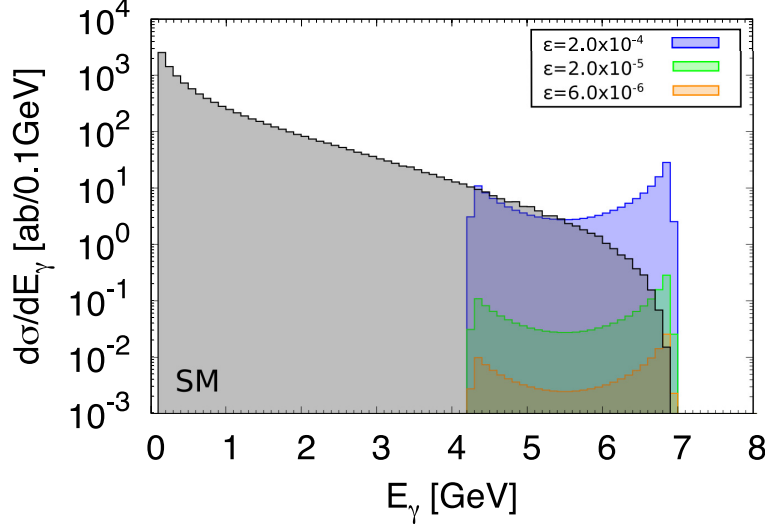


FIG. 3: The differential cross section of  $e^+ + e^- \rightarrow \gamma + Z'$  with respect to the photon energy,  $E_\gamma$ . The blue, green and the orange histograms correspond to  $\epsilon = 2 \times 10^{-4}$ ,  $2 \times 10^{-5}$  and  $6 \times 10^{-6}$ , respectively. The grey histogram represents the SM background.

where  $E_{e^\pm}$  is the energy of positron and electron, and  $\theta_\gamma$  is the angle between the photon momentum and the electron momentum. Here we ignored the angle between the positron and electron momenta for simplicity. The Belle-II detector can identify the photon for  $E_\gamma \geq 0.1$  GeV with the resolution 0.1 GeV and the angle  $15^\circ \leq \theta_\gamma \leq 135^\circ$  [72]. With these cuts, the photon energy ranges  $4.3 \leq E_\gamma \leq 6.9$  GeV.

Figure 3 shows the differential cross section of  $e^+ + e^- \rightarrow \gamma + Z'$  with respect to the photon energy,  $E_\gamma$ . The blue, green and the orange histograms correspond to  $\epsilon = 2 \times 10^{-4}$ ,  $2 \times 10^{-5}$  and  $6 \times 10^{-6}$ , respectively. The grey histogram represents the SM background of  $\gamma$ -missing events, which comes from  $e^+ + e^- \rightarrow \gamma + Z^* \rightarrow \gamma + \nu + \bar{\nu}$  and also t-channel  $W$  exchange one. The mass of  $Z'$  is fixed to 100 MeV, however the differential cross section is almost independent of the mass for  $m_{Z'} \lesssim 300$  MeV. It can be seen from the figure that the differential cross section of the  $Z'$  production is different from the SM background. The deviations from the background become significant as  $\epsilon$  becomes larger. The expected numbers of events in the last two bins are 1500, 15 and 1.4 for each  $\epsilon$ , respectively while that of the SM background is less than 1. Therefore the search for  $Z'$  will be possible even for  $\epsilon = 6 \times 10^{-6}$  by measuring the mono photon events with the  $E_\gamma \gtrsim 6.8$  GeV.

Figures 4 and 5 are the contour plots of the cross section of  $e^+ + e^- \rightarrow \gamma + Z'$  followed by  $Z' \rightarrow \nu + \bar{\nu}$  in the  $g'$ - $\epsilon$  plane, where the decay branching ratio of  $Z' \rightarrow \nu + \bar{\nu}$  is obtained from Eqs. (5). In each panel, the mass of  $Z'$  and the sign of  $\epsilon$  are the same as Figures 1 and 2, respectively. The dashed curves represent the contours of the cross section between 200 to 0.02 ab from top to bottom. Assuming the luminosity  $50 \text{ ab}^{-1}$ , the expected numbers of events to each cross sections are from  $10^4$  to 1. The grey regions are the excluded region in

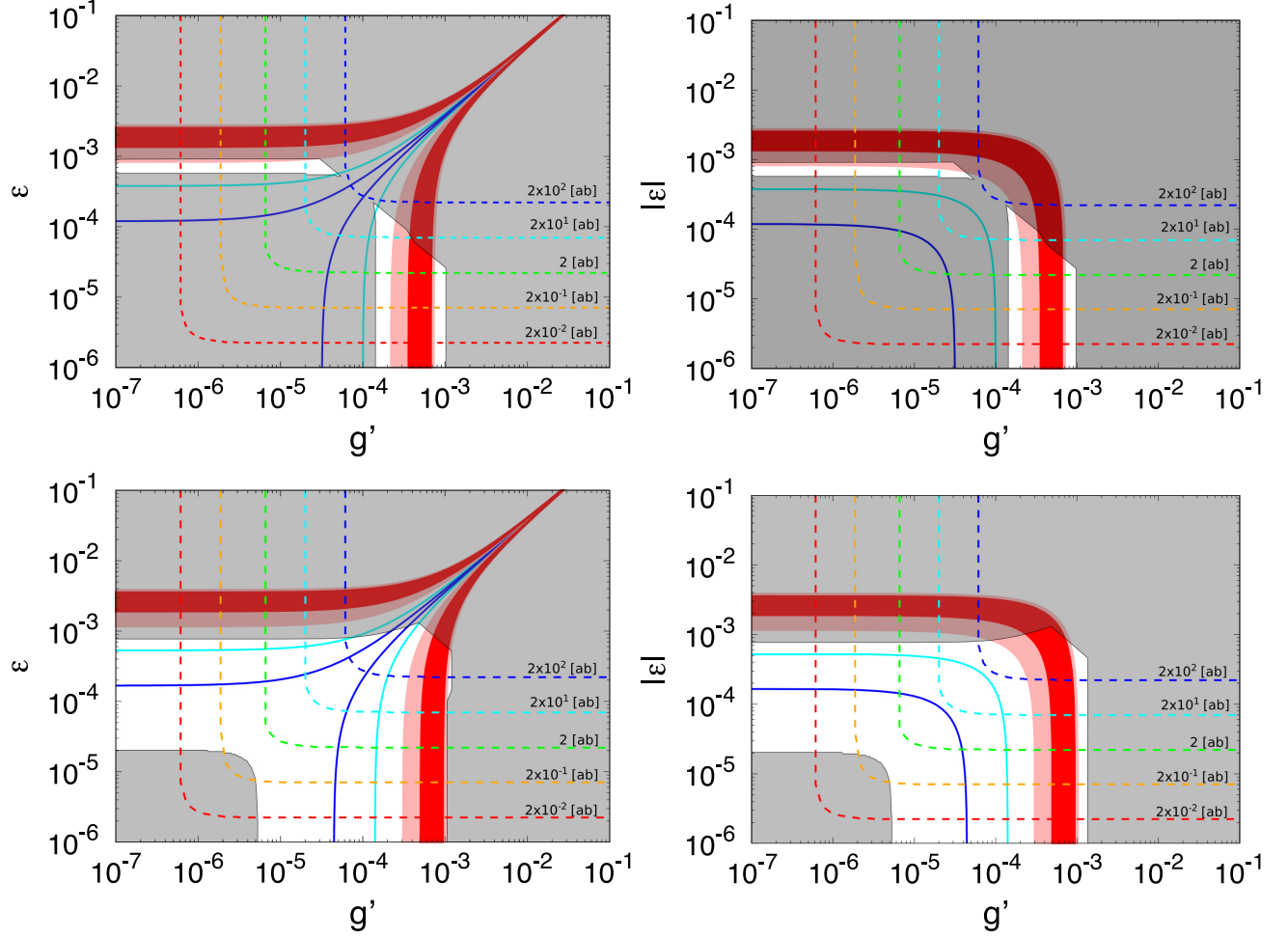


FIG. 4: The contour plots of the total cross section of  $e^+ + e^- \rightarrow \gamma + \nu + \bar{\nu}$  for 10 (top) and 50 (bottom) MeV. The left and right panels correspond to  $\epsilon > 0$  and  $\epsilon < 0$  cases, respectively. The numbers near each dashed curves are the cross sections in ab. The red and pink bands represent  $(g - 2)_\mu$  within  $2\sigma$  and  $3\sigma$ , and the solid cyan and blue curves represent  $\Delta a_\mu = 10^{-10}$  and  $10^{-11}$ , respectively.

Figs. 1 and 2, and the red and pink bands represent the favored regions of  $(g - 2)_\mu$  within  $2\sigma$  and  $3\sigma$ . The solid cyan and blue curves represent  $\Delta a_\mu = 10^{-10}$  and  $10^{-11}$  for references. When the planned experiments reduce the uncertainties and if the same-level progresses on theoretical side are made, such smaller contributions to  $(g - 2)_\mu$  might be required.

The shape of the contours can be understood as follows. The production cross section of  $Z'$  is proportional to  $\epsilon^2$  while the decay branching ratio is proportional to  $g'^2/(g'^2 + \epsilon^2 + \dots)$ . Thus, the total cross section is proportional to  $\epsilon^2 g'^2/(g'^2 + \epsilon^2 + \dots)$ . When  $\epsilon$  is much smaller than  $g'$ , the total cross section is independent of  $g'$ . In the opposite situation,  $\epsilon \gg g'$ , the cross section becomes independent of  $\epsilon$ . It is important to be noted here that the differential cross section with respect to  $E_\gamma$  is the same on each contour even if the branching ratio

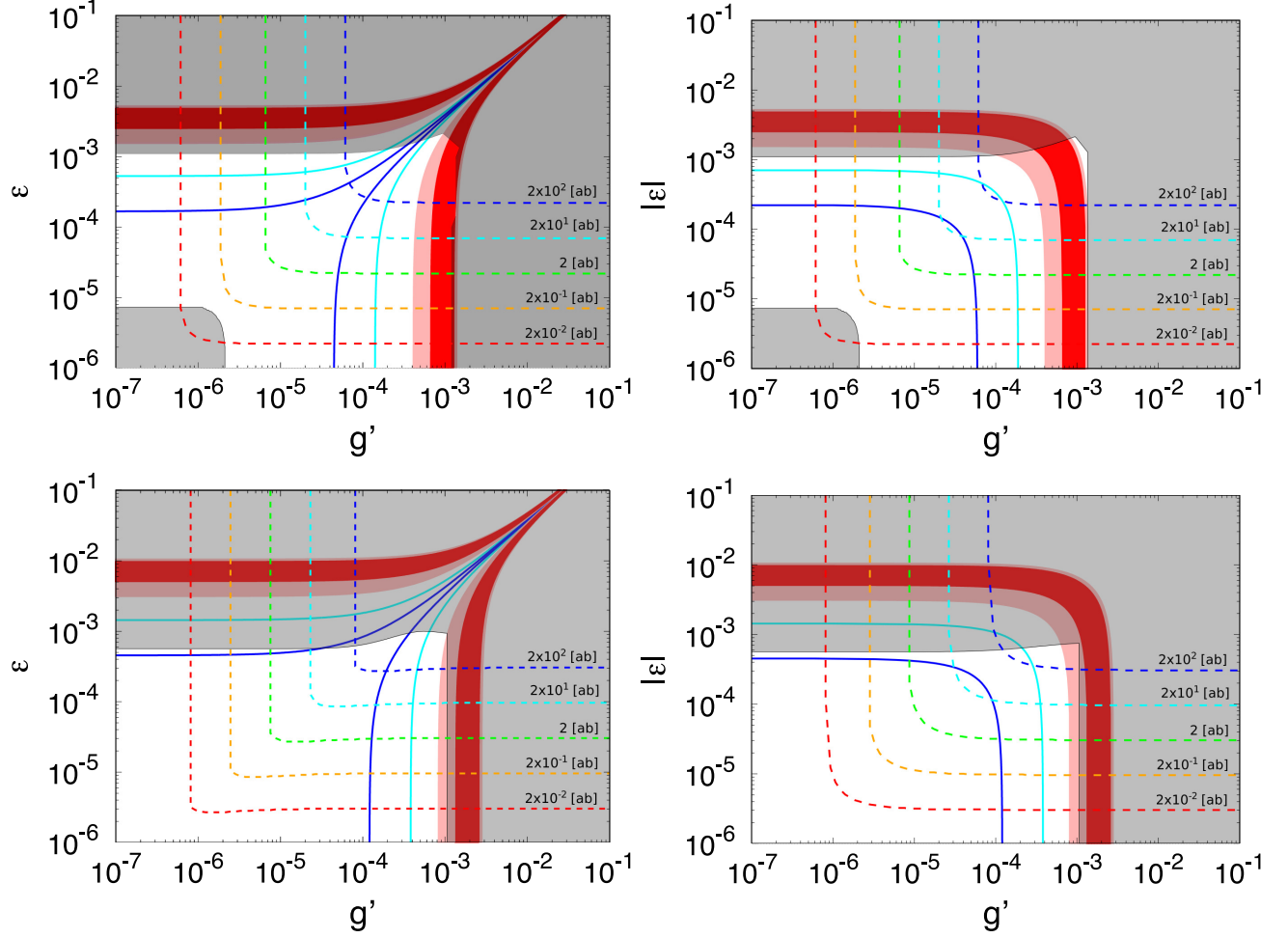


FIG. 5: The same plots as Figure 4 for  $m_{Z'} = 100$  (top) and 300 (bottom) MeV.

is different. This is because the shape of the different cross section is determined by the production cross section and the magnitude of that is determined by the total cross section.

The contour of 0.2 ab is close to the case of  $\epsilon = 6 \times 10^{-6}$  in figure 3. From the figures 4 and 5, it can be seen that the contour of 0.2 ab covers the region of  $g' \gtrsim 2 \times 10^{-6}$  and  $\epsilon \gtrsim 7 \times 10^{-6}$ . As discussed in Fig. 3, the signal is larger than the SM background and hence this region will be explored. Furthermore, the curves of  $\Delta a_\mu = 10^{-10}$  and  $10^{-11}$  are covered in this region. Therefore, not only the present  $(g-2)_\mu$  favored regions but also smaller ones can be examined by the Belle-II experiment.

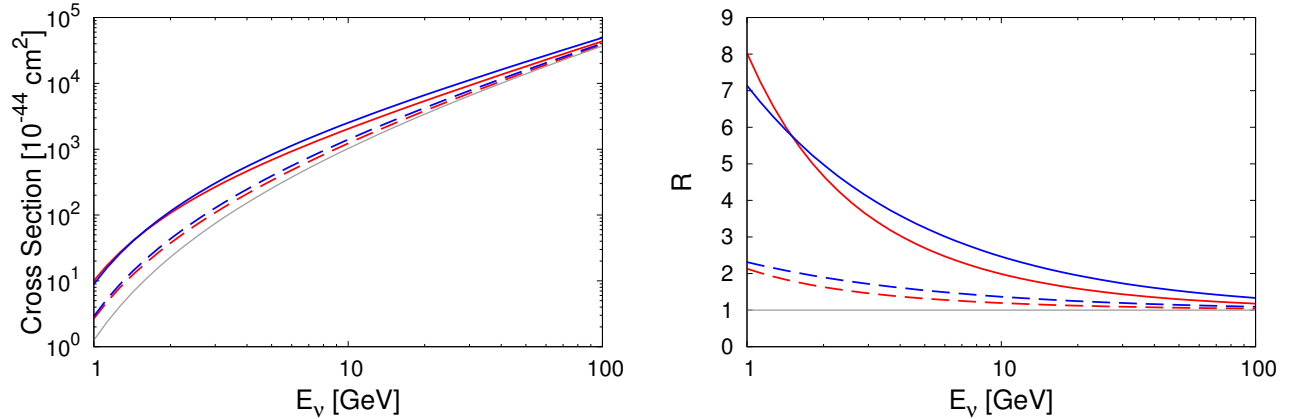


FIG. 6: The cross section of the neutrino trident production process (left) and the ratio of the cross section to the SM one,  $R$ , (right) in terms of the neutrino energy for an iron target. The kinetic mixing parameter is fixed to  $10^{-5}$ , and the  $Z'$  mass is taken to be 10 (red) and 100 (blue) MeV, respectively. The gauge coupling constant is taken as  $g' = 5.8 \times 10^{-4}$  (red-solid),  $3.4 \times 10^{-4}$  (red-dashed), and  $g' = 9.5 \times 10^{-4}$  (blue-solid),  $5.8 \times 10^{-4}$  (blue-dashed), respectively. The grey curve represents the SM cross section.

## B. Neutrino Beam Experiments

Next we discuss the detection possibilities of the  $Z'$  boson at neutrino beam experiments through the neutrino trident production process<sup>6</sup>.

Figure 6 shows the cross section of the neutrino trident production (left) in the  $L_\mu - L_\tau$  model and the SM, and the ratio of the cross section to the SM one,  $R$ , (right) in terms of the neutrino energy,  $E_\nu$ . We assume an iron target with the mass number 55.0 and the atomic number 26. The kinetic mixing parameter is fixed to  $\epsilon = 10^{-5}$ , and the mass is chosen as  $m_{Z'} = 10$  (red curves) and 100 (blue curves) MeV as reference values, respectively. The gauge coupling constant is taken to be  $g' = 5.8 \times 10^{-4}$  (red-solid),  $3.4 \times 10^{-4}$  (red-dashed), and  $g' = 9.5 \times 10^{-4}$  (blue-solid),  $5.8 \times 10^{-4}$  (blue-dashed), respectively. The grey curve represents the SM cross section. It is seen from the left panel that the trident production cross section becomes larger as the neutrino energy is larger. It reaches to  $(3.7-4.9) \times 10^{-40}$  cm<sup>2</sup> for  $E_\nu = 100$  GeV while it does to  $(0.12-1.0) \times 10^{-43}$  cm<sup>2</sup> at  $E_\nu = 1$  GeV. It is also seen from the right panel that the ratio  $R$  becomes larger as  $E_\nu$  is lower. This fact suggests that neutrino beams with lower energy have better sensitivity to search for the light  $Z'$  boson. The ratio is roughly larger than 2 for  $E_\nu \lesssim 1.5$  GeV for our reference parameters. Since the

<sup>6</sup> Some results in this subsection overlap with [30] which appeared on arXiv while our manuscript had been prepared. The results were presented at "The international workshop on future potential of high intensity accelerators for particle and nuclear physics (HINT2016)", at J-PARC, Tokai, Japan and other places.

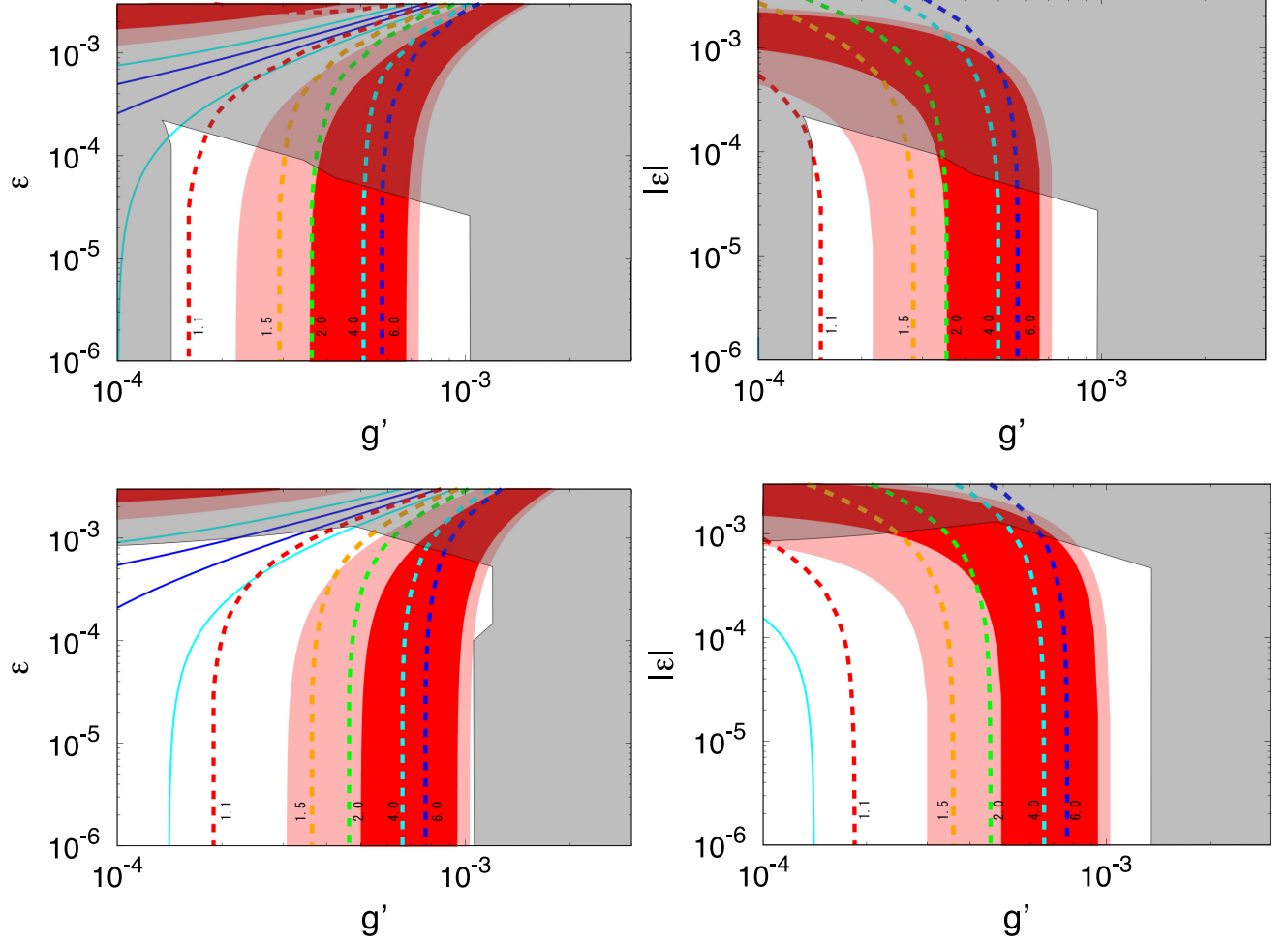


FIG. 7: The contour plot of  $R$  in the  $g'$ - $\epsilon$  plane for 10 (top) and 50 (bottom) MeV. The dashed curves represent  $R$  with the number indicated aside. The grey region, the red and pink bands and the solid curves are the same in Figure 4 and 5.

cross section becomes smaller for the lower energy beam, larger flux is inevitably needed to have enough events. For higher neutrino energies, such as DUNE [37] and SHiP [38], the detailed study can be found in [30].

In figures 7 and 8, the ratios of the cross section are shown for the same parameters of figures 1 and 2. The values of  $R$  are indicated near each curves. The energy of neutrino is taken to be 1.5 GeV which is the same energy at the INGRID detector at the T2K experiment [77]. One can see that the contour curves are different in the left and right panels for each  $m_{Z'}$ . As explained in Sec. IV, the difference originates from the relative phase between the amplitudes, and is significant for the lower neutrino energy. In the panels, it is seen that the region with  $g'$  smaller than from the present bound can be searched even for  $R \lesssim 6$  except for  $m_{Z'} = 300$  MeV. It is also seen that the same ratio as the CCFR experiment,  $R \lesssim 1.1$ , can provide the search for entire region of  $(g-2)_\mu$  within  $3\sigma$  for  $m_{Z'} \lesssim 300$  MeV and also

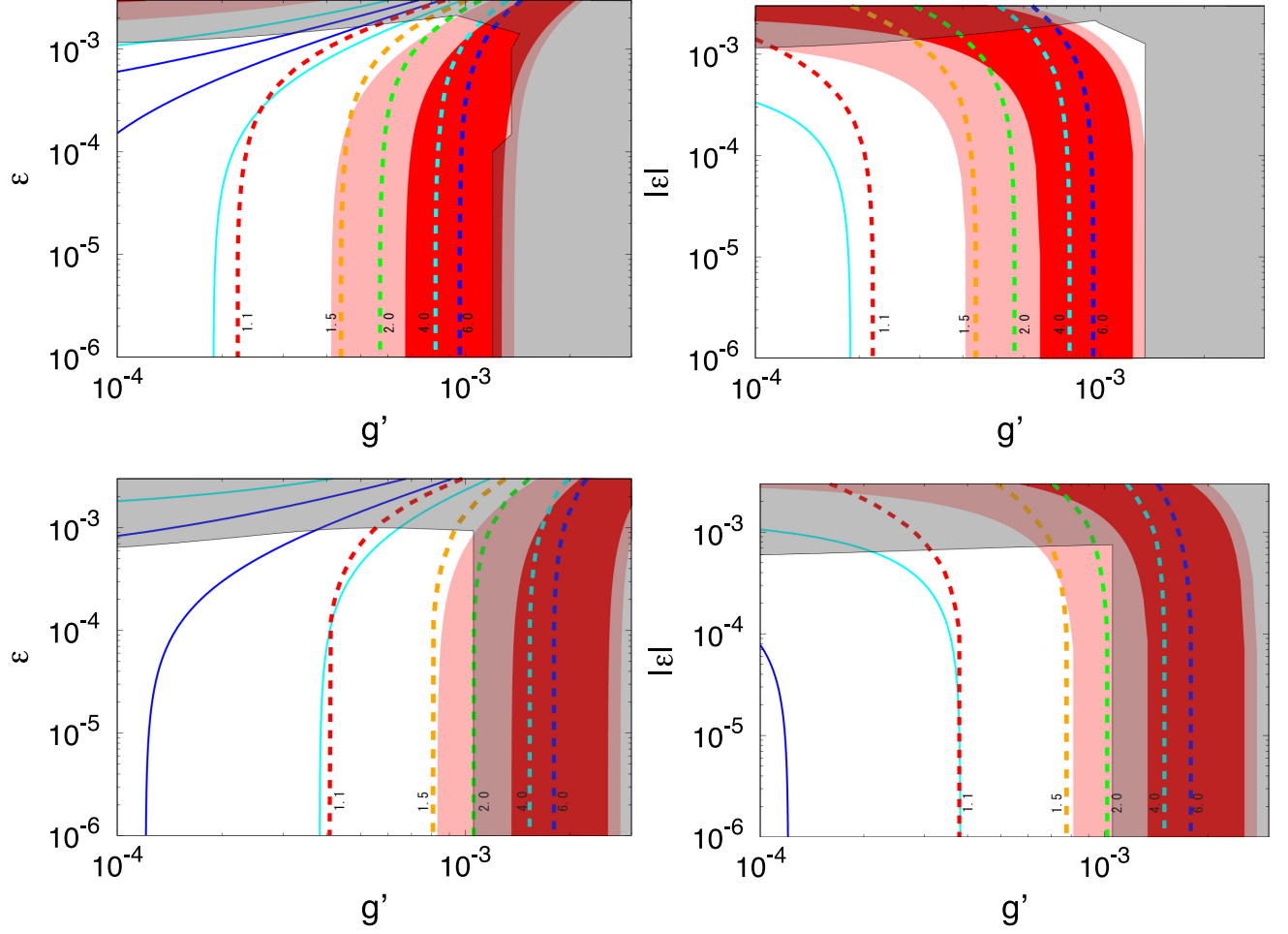


FIG. 8: The same plots with Figure 8 for 100 (top) and 300 (bottom) MeV.

some part of  $\Delta a_\mu = 10^{-10}$ .

As mentioned above and in Sec. IV, the  $Z'$  contribution to the trident production cross section can be positive or negative depending on  $\epsilon$ . In fact, when  $\epsilon > g' > 0$ , the  $Z'$  amplitude is negative and interferes destructively with the SM amplitude. Then, the ratio  $R$  can become smaller than the unity. This can not happen in the  $L_\mu - L_\tau$  model without the tree-level kinetic mixing because the loop induced kinetic mixing is always smaller than  $g'$ .

Figure 9 shows the  $\epsilon$  dependence of  $R$ . The mass of  $Z'$  is taken to be  $m_{Z'} = 50, 100$  and  $300$  MeV for the dotted, dashed and solid curves, and the coupling constant is taken to be  $g' = 10^{-4}$  and  $5 \times 10^{-4}$  for the red and blue ones, respectively. The neutrino energy is fixed to  $1.5$  GeV. It is seen that  $R$  gradually decreases as  $\epsilon$  increases, and then quickly increases after it reaches at a minimum. This behavior can be understood as follows. The interference term with the SM amplitude is proportional to  $g' - \epsilon \epsilon \cos \theta_W$  while the absolute square of the  $Z'$  amplitude is proportional to the square of that. Therefore the total cross



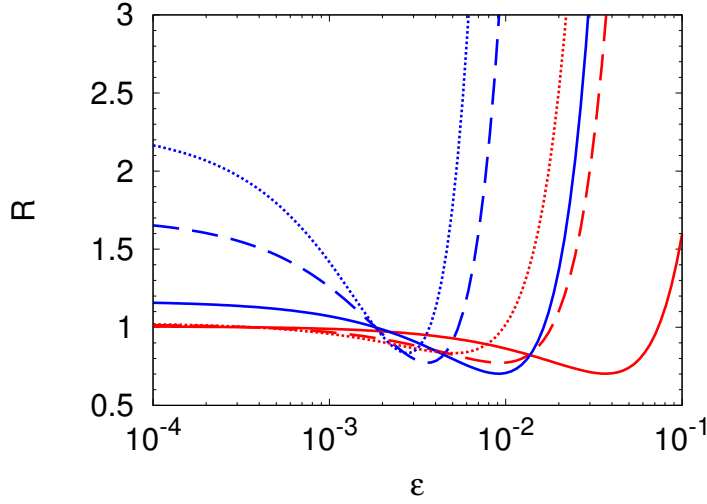


FIG. 9: The ratio of the cross sections,  $R$ , as a function of  $g'$ . The solid, dashed and dotted curves represent  $R$  for  $m_{Z'} = 300, 100$  and  $50$  MeV, and the red and blue ones for  $g' = 10^{-4}$  and  $5 \times 10^{-4}$ , respectively. The neutrino energy is fixed to  $E_\nu = 1.5$  GeV.

section decreases linearly in  $\epsilon$ . After reached at the minimum, the absolute squared term dominates over the interference term and the cross section increases quadratically in  $\epsilon$ . It is also seen that  $\epsilon$  at the minimum is larger as  $g'$  is smaller. Moreover, it can be seen that the minimum of  $R$  is smaller for larger  $m_{Z'}$  and is independent of  $g'$ . The minimum is easily obtained by minimizing the total cross section with respect to it, and is given by  $\epsilon_{\min} = \frac{1}{e \cos \theta_W} (g' + g'^{-1} \frac{A}{B})$  where  $A$  and  $B$  are independent of  $g'$  and  $\epsilon$ , and determined by the  $Z'$  amplitude. Then, using  $\epsilon_{\min}$ , the minimum of  $R$  is given by  $R_{\min} = 1 - \frac{A^2}{\sigma_{\text{SM}} B}$  where  $\sigma_{\text{SM}}$  stands for the SM cross section, which is independent of  $g'$  as well as  $\epsilon$ . Therefore, the minimum is determined only by  $m_{Z'}$  and  $E_\nu$ .

The neutrino trident production process is sensitive to the sign of  $\epsilon$  for  $|\epsilon| \gg g'$  while one photon plus missing search is insensitive to it. Thus, the neutrino beam experiment can provide the different information from the Belle-II experiment. For  $|\epsilon| \ll g'$ , the constraint becomes independent of  $\epsilon$ , and hence tight bounds can be set on it. On the other hand, the production cross section of  $Z'$  at  $e^+e^-$  colliders is proportional to  $\epsilon^2$  and hence it can not explore the small kinetic mixing region. Thus, the searches for the neutrino trident production process are complementary to the  $e^+e^-$  collider search, and are important to the search for the light and weakly interacting gauge boson.

## VI. SUMMARY AND DISCUSSION

We have considered the light and weakly interacting  $Z'$  boson in the gauged  $L_\mu - L_\tau$  model, simultaneously taking into account the gauge interaction and the kinetic mixing.

We studied the possibilities on the search for such the  $Z'$  boson analyzing one photon plus missing (neutrinos) events at the Belle-II experiment and the neutrino trident production process at neutrino beam experiments.

We have shown the allowed region in the  $g'$ - $\epsilon$  plane for  $m_{Z'} = 10, 50, 100$  and  $300$  MeV applying various experimental constraints and requirements. Then, the one photon plus missing events from  $Z'$  decay were analyzed in the allowed region. We showed that the differential cross section in terms of  $E_\gamma$  has an characteristic shape, and found the signal can be larger than the SM background for  $|\epsilon| > 6.0 \times 10^{-6}$  at least at the edge of  $E_\gamma$ . Thus, the search for the light  $Z'$  boson will be possible at the Belle-II experiment. We also showed the cross section for the parameter space in the  $g'$ - $\epsilon$  plane that can be explored at the Belle-II experiment.

For the neutrino trident production process, we showed that a neutrino beam with lower energy is more sensitive to the existence of  $Z'$ . Then, taking  $E_\gamma = 1.5$  GeV, the sensitivity was shown in the  $g'$ - $\epsilon$  plane. We found that even the ratio  $R \simeq 6$ , smaller parameters than the present bound can be explored. When the trident production cross section is measured more precisely, the whole region of  $(g - 2)_\mu$  favored region can be covered. We have shown that the neutrino trident production process is also sensitive to the sign of  $\epsilon$  while the one photon plus missing search is not. Therefore both experiments will be complementary in searching for the light  $Z'$  boson.

Before closing the summary, two comments are in order. 1) For the search at the Belle-II,  $e^+ + e^- \rightarrow \text{multi-}\gamma$  can also be serious backgrounds if several photons are undetected. The total cross sections of 2-, 3- and 4-gamma final states are roughly estimated as  $10^9$ ,  $10^8$  and  $10^6$  ab, respectively. Thus, the expected numbers of the these backgrounds would be much larger than that of the signal events. For two photon in the final state, changing the cut on the photon angle will reduce this background. However, for more photons case, it is not easy to reduce such the events, especially for the cases that only one photon is measured and other photons escape to beam directions. Therefore more detailed study on the background is needed to determine the parameter space to be explored. 2) For the neutrino trident production process, the momenta and angle distributions of the muons are important to discriminate the signal from the background. We leave these for our future works.

## Acknowledgments

The authors would like to thank K. Hayasaka and T. Yoshinobu for fruitful discussions and useful information on the Belle-II detector. Y.K would like to thank the visitor support program in Japan Particle and Nuclear Forum. The work of T.S is supported by JSPS

- [1] G. W. Bennett et al. (Muon g-2), Phys. Rev. **D73**, 072003 (2006), hep-ex/0602035.
- [2] C. Patrignani et al. (Particle Data Group), Chin. Phys. **C40**, 100001 (2016).
- [3] M. Davier, A. Hoecker, B. Malaescu, and Z. Zhang, Eur. Phys. J. **C71**, 1515 (2011), [Erratum: Eur. Phys. J. **C72**, 1874(2012)], 1010.4180.
- [4] F. Jegerlehner and R. Szafron, Eur. Phys. J. **C71**, 1632 (2011), 1101.2872.
- [5] K. Hagiwara, R. Liao, A. D. Martin, D. Nomura, and T. Teubner, J. Phys. **G38**, 085003 (2011), 1105.3149.
- [6] T. Aoyama, M. Hayakawa, T. Kinoshita, and M. Nio, Phys. Rev. Lett. **109**, 111808 (2012), 1205.5370.
- [7] M. Aoki et al., <http://g-2.kek.jp/portal/index.html>.
- [8] J. Grange et al. (Muon g-2) (2015), 1501.06858.
- [9] F. Jegerlehner and A. Nyffeler, Phys. Rept. **477**, 1 (2009), 0902.3360.
- [10] M. Lindner, M. Platscher, and F. S. Queiroz (2016), 1610.06587.
- [11] P. Fayet (2016), 1611.05357.
- [12] R. Foot, Mod. Phys. Lett. **A6**, 527 (1991).
- [13] R. Foot, X. G. He, H. Lew, and R. R. Volkas, Phys. Rev. **D50**, 4571 (1994), hep-ph/9401250.
- [14] X.-G. He, G. C. Joshi, H. Lew, and R. R. Volkas, Phys. Rev. **D44**, 2118 (1991).
- [15] S. Choubey and W. Rodejohann, Eur. Phys. J. **C40**, 259 (2005), hep-ph/0411190.
- [16] T. Ota and W. Rodejohann, Phys. Lett. **B639**, 322 (2006), hep-ph/0605231.
- [17] J. Heeck and W. Rodejohann, J. Phys. **G38**, 085005 (2011), 1007.2655.
- [18] J. Heeck and W. Rodejohann, Phys. Rev. **D84**, 075007 (2011), 1107.5238.
- [19] J. Heeck, M. Holthausen, W. Rodejohann, and Y. Shimizu, Nucl. Phys. **B896**, 281 (2015), 1412.3671.
- [20] A. Biswas, S. Choubey, and S. Khan (2016), 1612.03067.
- [21] A. Biswas, S. Choubey, and S. Khan, JHEP **09**, 147 (2016), 1608.04194.
- [22] M. G. Aartsen et al. (IceCube), Phys. Rev. Lett. **113**, 101101 (2014), 1405.5303.
- [23] T. Araki, F. Kaneko, Y. Konishi, T. Ota, J. Sato, and T. Shimomura, Phys. Rev. **D91**, 037301 (2015), 1409.4180.
- [24] A. Kamada and H.-B. Yu, Phys. Rev. **D92**, 113004 (2015), 1504.00711.
- [25] T. Araki, F. Kaneko, T. Ota, J. Sato, and T. Shimomura, Phys. Rev. **D93**, 013014 (2016), 1508.07471.
- [26] W. Altmannshofer, S. Gori, M. Pospelov, and I. Yavin, Phys. Rev. **D89**, 095033 (2014), 1403.1269.
- [27] W. Altmannshofer and I. Yavin, Phys. Rev. **D92**, 075022 (2015), 1508.07009.
- [28] W. Altmannshofer, S. Gori, S. Profumo, and F. S. Queiroz, JHEP **12**, 106 (2016), 1609.04026.

- [29] W. Altmannshofer, S. Gori, M. Pospelov, and I. Yavin, Phys. Rev. Lett. **113**, 091801 (2014), 1406.2332.
- [30] G. Magill and R. Plestid (2016), 1612.05642.
- [31] M. Ibe, W. Nakano, and M. Suzuki (2016), 1611.08460.
- [32] W. Altmannshofer, C.-Y. Chen, P. S. Bhupal Dev, and A. Soni, Phys. Lett. **B762**, 389 (2016), 1607.06832.
- [33] K. Harigaya, T. Igari, M. M. Nojiri, M. Takeuchi, and K. Tobe, JHEP **03**, 105 (2014), 1311.0870.
- [34] S. Patra, S. Rao, N. Sahoo, and N. Sahu (2016), 1607.04046.
- [35] J. Heeck (2016), 1610.07623.
- [36] S. N. Gninenko, N. V. Krasnikov, and V. A. Matveev, Phys. Rev. **D91**, 095015 (2015), 1412.1400.
- [37] R. Acciarri et al. (DUNE) (2015), 1512.06148.
- [38] M. Anelli et al. (SHiP) (2015), 1504.04956.
- [39] R. Essig, P. Schuster, and N. Toro, Phys. Rev. **D80**, 015003 (2009), 0903.3941.
- [40] R. Essig, J. Mardon, M. Papucci, T. Volansky, and Y.-M. Zhong, JHEP **11**, 167 (2013), 1309.5084.
- [41] V. V. Ezhela, S. B. Lugovsky, and O. V. Zenin (2003), hep-ph/0312114.
- [42] M. Davier, S. Eidelman, A. Hocker, and Z. Zhang, Eur. Phys. J. **C27**, 497 (2003), hep-ph/0208177.
- [43] S. R. Mishra et al. (CCFR), Phys. Rev. Lett. **66**, 3117 (1991).
- [44] D. Geiregat et al. (CHARM-II), Phys. Lett. **B245**, 271 (1990).
- [45] C. F. von Weizsacker, Z. Phys. **88**, 612 (1934).
- [46] E. J. Williams, Phys. Rev. **45**, 729 (1934).
- [47] A. Belyaev, N. D. Christensen, and A. Pukhov, Comput. Phys. Commun. **184**, 1729 (2013), 1207.6082.
- [48] R. W. Brown, R. H. Hobbs, J. Smith, and N. Stanko, Phys. Rev. **D6**, 3273 (1972).
- [49] R. Harnik, J. Kopp, and P. A. N. Machado, JCAP **1207**, 026 (2012), 1202.6073.
- [50] S. Bilmis, I. Turan, T. M. Aliev, M. Deniz, L. Singh, and H. T. Wong, Phys. Rev. **D92**, 033009 (2015), 1502.07763.
- [51] M. Deniz et al. (TEXONO), Phys. Rev. **D81**, 072001 (2010), 0911.1597.
- [52] H. B. Li et al. (TEXONO), Phys. Rev. Lett. **90**, 131802 (2003), hep-ex/0212003.
- [53] H. T. Wong et al. (TEXONO), Phys. Rev. **D75**, 012001 (2007), hep-ex/0605006.
- [54] J.-W. Chen, H.-C. Chi, H.-B. Li, C. P. Liu, L. Singh, H. T. Wong, C.-L. Wu, and C.-P. Wu, Phys. Rev. **D90**, 011301 (2014), 1405.7168.
- [55] G. Bellini et al., Phys. Rev. Lett. **107**, 141302 (2011), 1104.1816.
- [56] Z. Maki, M. Nakagawa, and S. Sakata, Prog. Theor. Phys. **28**, 870 (1962).
- [57] B. Pontecorvo, Sov. Phys. JETP **26**, 984 (1968), [Zh. Eksp. Teor. Fiz.53,1717(1967)].

- [58] H. Nunokawa, S. J. Parke, and R. Zukanovich Funchal, Phys. Rev. **D74**, 013006 (2006), hep-ph/0601198.
- [59] E. M. Riordan et al., Phys. Rev. Lett. **59**, 755 (1987).
- [60] J. Blumlein and J. Brunner, Phys. Lett. **B701**, 155 (2011), 1104.2747.
- [61] R. Essig et al., in *Proceedings, Community Summer Study 2013: Snowmass on the Mississippi (CSS2013): Minneapolis, MN, USA, July 29-August 6, 2013* (2013), 1311.0029, URL <https://inspirehep.net/record/1263039/files/arXiv:1311.0029.pdf>.
- [62] J. R. Batley et al. (NA48/2), Phys. Lett. **B746**, 178 (2015), 1504.00607.
- [63] S. Adler et al. (E787), Phys. Rev. **D70**, 037102 (2004), hep-ex/0403034.
- [64] A. V. Artamonov et al. (E949), Phys. Rev. Lett. **101**, 191802 (2008), 0808.2459.
- [65] D. Banerjee et al. (NA64) (2016), 1610.02988.
- [66] D. Babusci et al. (KLOE-2), Phys. Lett. **B720**, 111 (2013), 1210.3927.
- [67] D. Babusci et al. (KLOE-2), Phys. Lett. **B736**, 459 (2014), 1404.7772.
- [68] J. P. Lees et al. (BaBar), Phys. Rev. Lett. **113**, 201801 (2014), 1406.2980.
- [69] J. P. Lees et al. (BaBar), Phys. Rev. **D94**, 011102 (2016), 1606.03501.
- [70] G. F. Giudice, P. Paradisi, and M. Passera, JHEP **11**, 113 (2012), 1208.6583.
- [71] T. Aoyama, M. Hayakawa, T. Kinoshita, and M. Nio, Phys. Rev. **D91**, 033006 (2015), 1412.8284.
- [72] T. Abe et al. (Belle-II) (2010), 1011.0352.
- [73] E. Ma and J. Okada, Phys. Rev. Lett. **41**, 287 (1978), [Erratum: Phys. Rev. Lett.41,1759(1978)].
- [74] M. Carena, A. de Gouvea, A. Freitas, and M. Schmitt, Phys. Rev. **D68**, 113007 (2003), hep-ph/0308053.
- [75] P. Fayet, Phys. Rev. **D75**, 115017 (2007), hep-ph/0702176.
- [76] B. Aubert et al. (BaBar), in *Proceedings, 34th International Conference on High Energy Physics (ICHEP 2008): Philadelphia, Pennsylvania, July 30-August 5, 2008* (2008), 0808.0017, URL <http://www-public.slac.stanford.edu/sciDoc/docMeta.aspx?slacPubNumber=slac-pub-13328>.
- [77] K. Abe et al. (T2K), Nucl. Instrum. Meth. **A659**, 106 (2011), 1106.1238.